



# Modeling and analysis of HVOF thermal spray process accounting for powder size distribution

Mingheng Li, Panagiotis D. Christofides\*

*Department of Chemical Engineering, University of California, 405 Hilgard Avenue Box 951592, Los Angeles, CA 90095-1592, USA*

## Abstract

This work focuses on the high velocity oxygen–fuel (HVOF) thermal spray processing of coatings and presents a fundamental model for the process which explicitly accounts for the effect of powder size distribution. The model describes the evolution of the gas thermal and velocity fields, as well as the motion and temperature of agglomerate particles of different sizes. In addition to providing useful insight into the in-flight behavior of particles with different sizes, the model is used to make a control-relevant parametric analysis of the HVOF thermal spray process. This analysis allows us to systematically characterize the influence of controllable process variables such as combustion chamber pressure, oxygen/fuel ratio, as well as the effect of powder size distribution, on the values of particle velocity and temperature at the point of impact on substrate. Specifically, the study shows that particle velocity is primarily influenced by the combustion chamber pressure, and particle temperature is strongly dependent on the fuel/oxygen ratio. Furthermore, it shows that the particle velocity and temperature at the point of impact depend strongly on particle size. These findings are consistent with available experimental observations and set the basis for the formulation of the control problem for the HVOF process.

© 2003 Elsevier Science Ltd. All rights reserved.

*Keywords:* HVOF thermal spray; Coatings processing; Powder size distribution; Modeling and analysis

## 1. Introduction

The high velocity oxygen–fuel (HVOF) thermal spray technology is widely used in the automotive and aerospace industry to deposit coatings. Using the thermal energy produced by the combustion of fuel with oxygen to heat and propel the spray particles, it provides a highly efficient way to modify the surface properties of the substrate to extend product life, increase performance and reduce maintenance costs. Recently, there is an increasing interest in the HVOF thermal spray processing of nanostructured coatings, whose grain size is less than about 100 nm (Lau, Jiang, Nuchter, & Lavernia 1998). This interest has been motivated by several factors, including: (1) the cost-effective production of high-quality nanosize powders, and (2) the discovery that nanostructured coatings exhibit superior qualities over traditional counterparts (made of materials with micro-sized grains) in several aspects including hardness, strength, ductility and diffusivity (Tellkamp, Lau, & Lavernia, 1997).

HVOF thermal spray provides an efficient way for depositing coatings of nanostructured materials because: (1) the powder particles hit the substrate with relatively high speed, which produces coatings with high density and high hardness, and (2) relatively low gas temperature prevents particles from being superheated during flight and helps to preserve the nanocrystalline structure of powders deposited on the substrate.

Over the last decade, the need to optimally design and operate thermal spray processes has motivated significant research on the development of fundamental mathematical models to explicitly account for the various physicochemical phenomena and to describe the dynamic behavior of various process components. Specifically, fundamental models have been developed describing the gas dynamics and particle in-flight behavior inside of the HVOF gun and in the free jet; molten drop deposition, solidification and microstructure development; and the relationship between coating microstructure and mechanical properties; the reader may refer to (Cheng, Trapaga, McKelliget, & Lavernia, 2001a) for an overview of results on mathematical modeling.

Despite the recent progress of numerical modeling of HVOF process, the effect of powder size distribution on

\* Corresponding author. Tel.: +1-310-794-1015; fax: +1-310-206-4107.

*E-mail address:* [pdc@seas.ucla.edu](mailto:pdc@seas.ucla.edu) (P.D. Christofides).

particle velocity and temperature, has not been studied. Motivated by the fact that the powders used in the HVOF process are polydisperse and the averaged particle properties are more significant than those defined on the basis of an individual particle, we present a mathematical model for the HVOF process which explicitly accounts for the effect of powder size distribution. In addition to providing useful insight into the in-flight behavior of particles with different sizes, the model is used to make a parametric analysis of the HVOF process. This analysis allows us to systematically characterize the influence of controllable process variables such as combustion chamber pressure, oxygen/fuel ratio, as well as the effect of powder size distribution, on the values of particle velocity and temperature at the point of impact on substrate. Specifically, the study shows that particle velocity is primarily influenced by the combustion chamber pressure, and particle temperature is strongly dependent on the fuel/oxygen ratio. Furthermore, it shows that the particle velocity and temperature at the point of impact depend strongly on particle size. These findings are consistent with available experimental observations and set the basis for the formulation of the control problem for the HVOF process.

## 2. Modeling of the HVOF process

### 2.1. Process description

Fig. 1 shows the schematic diagram of a commonly used HVOF thermal spray system. It consists of a combustion chamber, a de Laval nozzle (also known as convergent/divergent nozzle), and a barrel. High pressure and high temperature combustion gases, which are generated by the combustion of fuel gases (typically propylene, propane and hydrogen, etc.) with air in the combustion chamber, are accelerated to supersonic velocity through a de Laval nozzle. Outside of the gun, the supersonic free jet adjusts to the ambient pressure by a series of compression and expansion waves, and visible shock diamonds are formed downstream of the barrel exit due to the luminescence of various gases at high temperature. The powders are injected axially into the gas stream at the exit of the nozzle, where the pressure is not so high as that in the combustion chamber so that powders can easily enter the

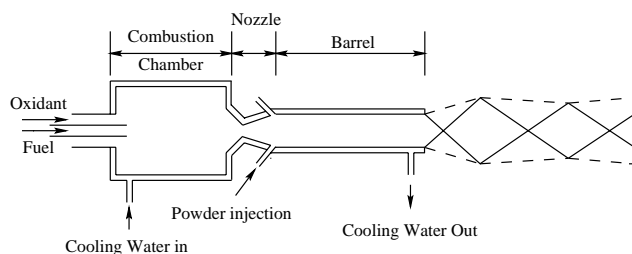


Fig. 1. Schematic of the HVOF flow field.

gas stream. After accelerated and heated in the barrel and in the free jet, the powders impinge on the substrate with high velocity to make coatings.

The HVOF thermal spray process features high gas/particle velocities and relatively low gas/particle temperatures, as compared with plasma spraying (Cheng, Trapaga, McKelliget, & Lavernia, 2001a). These unique process characteristics contribute to the superior qualities of coatings made with the HVOF process. On the one hand, spraying powders hitting the substrate with high speed tends to produce coatings with high density and high hardness. On the other hand, relatively low gas temperature prevents particles from being superheated during flight and help to preserve the nanocrystalline structure of powders deposited on the substrate.

From a modeling point of view, HVOF is a complex process which involves combustion, two phase turbulent compressible flow, heat transfer and supersonic/subsonic flow transitions. To be able to develop a fundamental model for this process that is computationally tractable and capable of capturing the main features of the process, we assume in this paper that the presence of particles has a negligible effect on the gas velocity and temperature field. This assumption is standard and reasonably valid because the particle loading, which is defined as the ratio of mass flow rate of particles to that of gases, is typically less than 4% (Yang & Eidelman, 1996). As a consequence, the two-phase problem can be decoupled so that the gas field can be solved first, followed by the simulation of particle inflight behavior. To further simplify the analysis, we also make the following standard assumptions: (1) the flame gas obeys the ideal gas law; (2) species reach equilibrium in the combustion chamber and the composition of the combustion products is frozen at the combustion condition along the de Laval nozzle and barrel due to the very short residence time of combustion gases in the HVOF gun; (3) the combustion gases behave like a perfect gas during isentropic compression and expansion, and the ratio of specific heat at constant pressure to that at constant volume ( $c_p/c_v$ ) is nearly a constant; and (4) the friction and cooling water effects along the nozzle and barrel are negligible so that laws of isentropic flow of compressible fluids apply. The assumption of frozen flow is validated in (Swank, Fincke, Haggard, & Irons, 1994a), which reveals that the combustion products are far from chemical equilibrium, because the values of gas enthalpy, temperature and velocity at the exit of gun barrel as predicted by numerical simulations with the instantaneous equilibrium model are significantly higher than the experimentally measured values (Swank et al., 1994a). Based on the fact that the flow during the de Laval nozzle is close to frozen rather than in equilibrium, it is suggested in Swank et al. (1994a) that a one-dimensional model with chemical equilibrium in the combustion chamber and frozen composition flow during the nozzle and barrel should give a more accurate prediction than the one with instantaneous equilibrium flow. Frozen flow means that the gas residence time is much shorter than

the chemical kinetics such that the composition of the combustion gases during the nozzle and the gun barrel is the same as the one in the combustion chamber.

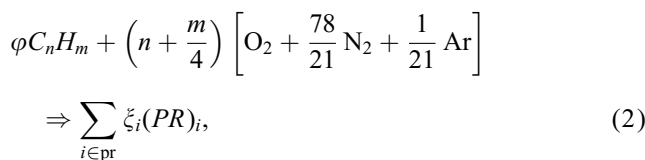
As shown in Fig. 1, the computational domain includes the combustion chamber, the de Laval nozzle and the barrel in the internal field and the supersonic free jet in the external field. There are four important cross sections involved in the internal field: the injection interface (inj), the combustion end (*c*), the nozzle throat (*t*) and the nozzle exit (*e*), which will be discussed later. The modeling procedure is that, for a given combustion chamber pressure (dependent on the total gas flow rate), and fuel/oxygen ratio, we first calculate the chemical composition in the combustion chamber, and then solve the gas properties along the nozzle, in the gun barrel and in the free jet in sequence. The profiles of particle velocity and temperature in the barrel and in the free jet are solved using the momentum transfer equation and the heat transfer equation.

## 2.2. Modeling of gas flow and thermal fields

To calculate the equilibrium composition in the combustion chamber, the fuel/oxygen ratio needs to be specified first. In practice, this term is usually expressed by the equivalence ratio:

$$\varphi = \frac{\text{fuel/oxygen}}{(\text{fuel/oxygen})_{\text{st}}}, \quad (1)$$

which is the actual fuel/oxygen ratio divided by the stoichiometric (denoted by the subscript *st*) fuel/oxygen ratio. The reactive system is fuel rich if  $\varphi > 1$  and fuel lean if  $\varphi < 1$ . Based on this definition, the reaction of a hydrocarbon fuel and air can be represented by a general equation of the form:



where *pr* represents products and  $\xi_i$  is the molar fraction of component *i* in the combustion products (*pr*), which include CO<sub>2</sub>, H<sub>2</sub>O and inert species (N<sub>2</sub> and Ar), and possibly CO, O<sub>2</sub> (depending on the value of the equivalence ratio). Under normal conditions, the reaction products do not include C<sub>n</sub>H<sub>m</sub>.

The equilibrium composition and temperature at the injection interface of the chamber can be calculated by minimizing the Gibbs free energy of the whole reactive system. This approach is advantageous compared to the equilibrium constant method because it does not require *a priori* specify a set of reactions (Gordon & McBride, 1994). Under the assumptions of adiabatic reaction and ideal gas behavior, the calculation of equilibrium composition in the combustion chamber can be formulated as an optimization problem

of the following form:

$$\begin{aligned} \min G &= \sum_{i \in \text{pr}} \mu_i \xi_i \\ \sum_{i \in \text{pr}} a_{ij} \xi_i &= b_j \quad (\forall j \in l) \\ \sum_{i \in \text{re}} \xi_i H_i^\theta(T_a) &= \sum_{j \in \text{pr}} \xi_j H_j^\theta(T_{\text{inj}}) \\ \mu_i &= \mu_i^\theta(T_{\text{inj}}) + RT_{\text{inj}} \ln \frac{P_{\text{inj}} \xi_i}{P^\theta \sum_{i \in \text{pr}} \xi_i}, \end{aligned} \quad (3)$$

where *G* is the Gibbs energy of the reactive system; *H<sub>i</sub>* and  $\mu_i$  are the enthalpy and chemical potential of species *i*, respectively; *T<sub>a</sub>* and *T<sub>inj</sub>* represent the ambient temperature and chamber temperature, respectively; superscript  $\theta$  represents the standard condition; *a<sub>ij</sub>* is the number of element *j* in species *i*, *b<sub>j</sub>* the sum of the number of element *j* in each molecule of reactants and *l* is the total number of chemical elements involved in the system; *R* is the gas constant and *P* is the pressure. The first equation listed in the constraints is the mass balance of each element involved in the reactive system, the second one is the energy balance, and the third one is the definition of chemical potential for ideal gases. Usually, the heat capacity of each species can be correlated as a polynomial of temperature and the enthalpy is derived as the integral of heat capacity with respect to temperature. If the oxidant used in the HVOF process is pure oxygen instead of air, a similar procedure can be followed.

For the compressible frozen flow in the internal flow field, the governing equations include continuity, momentum balance and energy balance. In particular, the momentum balance between the injection interface and the combustion end has the following form:

$$(P + \rho u^2)_{\text{inj}} = (P + \rho u^2)_c \quad (4)$$

and the energy balance equation is

$$\begin{aligned} \sum_{i \in \text{pr}} \xi_i H_i^\theta(T_{\text{inj}}) + \frac{1}{2} \left( \bar{M}_{\text{pr}} \sum_{i \in \text{pr}} \xi_i \right) u_{\text{inj}}^2 \\ = \sum_{i \in \text{pr}} \xi_i H_i^\theta(T_c) + \frac{1}{2} \left( \bar{M}_{\text{pr}} \sum_{i \in \text{pr}} \xi_i \right) u_c^2, \end{aligned} \quad (5)$$

where *u* is the gas velocity and  $\bar{M}_{\text{pr}}$  is the average molecular weight of the product. In supersonic flow, the gas velocity can be expressed by the following formula:

$$u = \mathbf{M} \mathbf{a} = \mathbf{M} \sqrt{\gamma P / \rho}, \quad (6)$$

where  $\rho$  is the gas density, **M** is the mach number which is defined as the ratio of the gas velocity to the local sonic velocity and  $\gamma$  is the adiabatic constant calculated by  $\gamma = \bar{c}_p / (\bar{c}_p - R)$ .

During the subsonic/supersonic transition, gases obtain sonic velocity at the throat of the Laval nozzle (i.e., the mach number at the throat, **M<sub>t</sub>**, is one). For isentropic flow

along the Laval nozzle, the relationship between area ratio and mach number at two cross sections is determined by

$$\frac{A_2}{A_1} = \frac{\mathbf{M}_1}{\mathbf{M}_2} \left\{ \frac{1 + [(\gamma - 1)/2]\mathbf{M}_2^2}{1 + [(\gamma - 1)/2]\mathbf{M}_1^2} \right\}^{(\gamma+1)/2(\gamma-1)}, \quad (7)$$

where  $A$  is the cross area perpendicular to the flow direction. For a nozzle with specific configuration, the mach number at the combustion end and the mach number at the nozzle exit can be solved based on the known area ratios  $A_c/A_t$  and  $A_e/A_t$  (see Fig. 1). Note that the same area ratio corresponds to two mach numbers, with one larger than 1 and the other less than 1, and therefore, an appropriate initial guess should be chosen to get the right solution when Newton–Raphson iteration is used.

Combining Eqs. (4)–(7) with the ideal gas law, and ignoring  $u_{inj}$ , one can solve for the gas properties such as velocity, temperature, pressure, and mach number at the combustion end. Then, the following relationships for isentropic compressible flow, together with Eq. (7), can be applied to compute the gas properties at other cross sections along the nozzle:

$$\frac{T_2}{T_1} = \frac{1 + [(\gamma - 1)/2]\mathbf{M}_1^2}{1 + [(\gamma - 1)/2]\mathbf{M}_2^2}, \quad (8)$$

$$\frac{P_2}{P_1} = \left\{ \frac{1 + [(\gamma - 1)/2]\mathbf{M}_1^2}{1 + [(\gamma - 1)/2]\mathbf{M}_2^2} \right\}^{\gamma/(\gamma-1)}, \quad (9)$$

$$\frac{\rho_2}{\rho_1} = \left\{ \frac{1 + [(\gamma - 1)/2]\mathbf{M}_1^2}{1 + [(\gamma - 1)/2]\mathbf{M}_2^2} \right\}^{1/(\gamma-1)}. \quad (10)$$

The above equations are derived from the governing equations for isentropic compressible flow and the reader may refer to the book (Roberson & Crowe, 1997) for a detailed derivation. The mass flow rate through a Laval nozzle, denoted by  $\dot{m}_g$ , can be approximately calculated by the following expression:

$$\dot{m}_g = \frac{P_{inj}}{\sqrt{T_{inj}}} A_t \sqrt{\frac{\bar{M}_{pr}}{R}} \gamma \left( \frac{2}{\gamma + 1} \right)^{(\gamma+1)/(\gamma-1)}. \quad (11)$$

Note that  $\dot{m}_g$  depends on the temperature and pressure in the chamber.

Under the assumptions of negligible friction and cooling water effects, the gas properties can be considered constant in the barrel. However, the exhaust gas cannot maintain the high velocity and temperature in the free jet (Jiang & Sislian, 1998; Cheng, Wehrmeyer, Pitz, Jarrett, & Northam, 1994). From the exit of the gun to a position whose distance is not larger than the potential core length ( $L_{pc}$ ), the gas velocity and temperature can be considered almost constant (Tawfik & Zimmerman, 1997). Further downstream, gas velocity and temperature decay rapidly because of the entrainment of the surrounding air; this decay can be adequately captured by

the following empirical formulae (Tawfik & Zimmerman, 1997):

$$\frac{u}{u_e} = 1 - \exp\left(\frac{0.85}{1 - x/L_{pc}}\right) \quad (12)$$

and

$$\frac{T - T_a}{T_e - T_a} = 1 - \exp\left(\frac{1.25}{1 - x/L_{pc}}\right), \quad (13)$$

where  $x$  is the axial distance from the exit of the gun barrel ( $x > L_{pc}$ ) and  $L_{pc}$  can be correlated to a function of the mach number at the exit of gun barrel ( $\mathbf{M}_e$ ) and barrel diameter ( $D$ )

$$L_{pc}/D = 3.5 + 1.0\mathbf{M}_e^2. \quad (14)$$

The above formulae are valid for  $1.5 \leq \mathbf{M}_e \leq 2.5$ ,  $1500 \text{ K} \leq T_e \leq 3000 \text{ K}$ .

### 2.3. Modeling of particle motion/temperature

The particle trajectories and temperature histories in the gas field are computed by the momentum and heat transfer equations. Because the acceleration and deceleration of particles in the moving gas in the HVOF thermal spray system are dominated by the drag force (Pawlowski, 1995), the particle motion can be described by the following two first-order ordinary differential equations:

$$\begin{aligned} m_p \frac{dv_p}{dt} &= \frac{1}{2} C_D \rho_g A_p (v_g - v_p) |v_g - v_p|, & v_p(0) &= 0, \\ \frac{dx_p}{dt} &= v_p, & x_p(0) &= 0. \end{aligned} \quad (15)$$

where  $v_p$  is the particle axial velocity,  $A_p$  is the projected area of the particle on the plane perpendicular to the flow direction,  $C_D$  is the drag coefficient, and  $x_p$  is the particle position, calculated from the exit of the nozzle. Note that one difference between particle motion in a stagnant fluid and particle motion in a moving fluid is that there is an absolute sign on the relative velocity between particle and gas in the latter case, which guarantees that a particle is accelerated if its velocity is less than that of the gas and decelerated otherwise.

To take into consideration the fact that the powders used in the HVOF process are not spherical (Cheng et al., 2001b), a formula for the drag coefficient ( $C_D$ ), which accounts for particle non-spherical shape using the so-called sphericity coefficient ( $\phi$ ) (defined as the ratio of the surface area of a sphere with equivalent volume to the actual surface area of the particle) is used in this paper (Ganser, 1993; Cheng et al., 2001b):

$$\begin{aligned} \frac{C_D}{K_2} &= \frac{24}{ReK_1K_2} [1 + 0.1118(ReK_1K_2)^{0.6567}] \\ &+ \frac{0.4305}{1 + 3305/ReK_1K_2}, \end{aligned} \quad (16)$$

where  $K_1$  and  $K_2$  are the Stokes' shape factor and the Newton's factor, respectively, which can be determined by

$$K_1^{-1} = \frac{1}{3} + \frac{2}{3\sqrt{\phi}}$$

$$\log(K_2) = 1.8148(-\log \phi)^{0.5743} \quad (17)$$

for isometric shapes. The local Reynolds number ( $Re$ ) is defined based on the relative velocity

$$Re = \frac{d_p |v_g - v_p| \rho_g}{\eta_g}, \quad (18)$$

where  $\eta_g$  is the gas viscosity and  $d_p$  is either the particle diameter if the particle is spherical or the equivalent diameter if not.

In the HVOF process, the particle Biot number ( $Bi = hx/\lambda_p$ ,  $h$  is the heat transfer coefficient,  $x$  is a characteristic dimension defined by the ratio of particle volume to its surface area, and  $\lambda_p$  is the thermal conductivity of the particle) is typically less than 0.1 (Cheng et al., 2001b). This means that particles are heated with negligible internal resistance and temperature gradients inside the particles can be ignored (Geankoplis, 1993). Consequently, the equation describing the heat transfer between a single particle and the gas reduces to a first-order ordinary differential equation of the form:

$$m_p c_p \frac{dT_p}{dt} = hA'_p(T_g - T_p), \quad T_p(0) = T_0, \quad (19)$$

where  $T_p$  is the particle temperature,  $m_p$  is the particle mass,  $A'_p$  is the surface area of a particle and  $h$  is the heat transfer coefficient computed by the Ranz–Marshall empirical equation (Bird, Stewart, & Lightfoot, 1960):

$$\frac{hd_p}{\lambda_g} = Nu = 2 + 0.65Re^{1/2}Pr^{1/3} \quad (20)$$

where the Prandtl number ( $Pr$ ) is calculated by  $Pr = c_p \eta_g / \lambda_g$ .

The equations for particle motion and particle temperature are solved by numerical integration. At each step, we integrate Eqs. (15) and (19) with a small enough time step such that the gas velocity, gas temperature, the local Reynolds number, and Prandtl number can all be considered constant over this interval. After one integration step, we update the gas velocity and gas temperature according to the new particle position and then apply the same strategy for the next time step. This methodology was proposed in Crowe and Stock (1976) and was found to be computationally economical and accurate. Specifically, the iterative formulae for particle velocity, position and temperature are:

$$v_p^{i+1} = v_g^i - (v_g^i - v_p^i) \exp(-\Delta t / \tau_p),$$

$$x_p^{i+1} = x_p^i + v_p^i \Delta t,$$

$$T_p^{i+1} = T_g^i - (T_g^i - T_p^i) \exp(-\Delta t / \omega_p), \quad (21)$$

where  $\tau_p = 4\rho_p d_p^2 / 3\eta_g C_D Re$  and  $\omega_p = \rho_p c_p d_p^2 / 6Nu\lambda_g$ .

#### 2.4. Modeling of powder size distribution

The powders used in the HVOF process are polydisperse. Recently, experimental work (e.g. Lavernia & Wu, 1996) has shown that lognormal functions can adequately describe many powders used in the HVOF process. To this end, we use a lognormal function to describe the powder size distribution of the form (Crow & Shimizu, 1988):

$$f(d_p) = \frac{1}{\sqrt{2\pi}\sigma d_p} \exp\left[-\frac{(\ln d_p - \mu)^2}{2\sigma^2}\right], \quad (22)$$

where  $f(d_p)$  is the size distribution function,  $\mu$  and  $\sigma^2$  are two dimensionless parameters corresponding to the mean and the variance of  $\ln d_p$ , which obeys the normal distribution. For particles that are lognormally distributed, the cumulative volume or weight function is defined as

$$F(d_p) = \frac{\int_0^{d_p} \frac{1}{6} \pi \rho d_p^3 f(d_p) d(d_p)}{\int_0^\infty \frac{1}{6} \pi \rho d_p^3 f(d_p) d(d_p)}$$

$$= \int_{-\infty}^{\frac{\ln d_p - (\mu + 3\sigma^2)}{\sigma}} \frac{1}{\sqrt{2\pi}} e^{-\frac{x^2}{2}} dx. \quad (23)$$

Once the value of  $F(d_p)$  is specified, the upper bound of the above integral can be found from standard integration tables. In experimental powder measurements,  $d_{10}$ ,  $d_{50}$  and  $d_{90}$ , which denote the particle sizes corresponding to 10%, 50% and 90% of the cumulative weight function, can be determined using a Microtrac Standard Range Particle Analyzer (Lau et al. 1998). When there are three sets of data available, parameter estimation can be applied by minimizing the square sum of differences between experimental data and theoretical predictions, i.e.

$$\min\{g\} = [\ln d_{10} - (\mu + 3\sigma^2) + 1.28\sigma]^2$$

$$+ [\ln d_{50} - (\mu + 3\sigma^2)]^2$$

$$+ [\ln d_{90} - (\mu + 3\sigma^2) - 1.28\sigma]^2. \quad (24)$$

The solution to the above minimization problem yields

$$\mu = \ln \sqrt[3]{d_{10} d_{50} d_{90}} - 1.831 \left( \ln \sqrt{\frac{d_{90}}{d_{10}}} \right)^2,$$

$$\sigma = 0.781 \ln \sqrt{\frac{d_{90}}{d_{10}}}. \quad (25)$$

Finally, the volume- or weight-based average of powder properties ( $PP$ ) can be calculated from the following equation:

$$\overline{PP} = \frac{\int_0^\infty \frac{1}{6} \pi \rho d_p^3 PP(d_p) f(d_p) d(d_p)}{\int_0^\infty \frac{1}{6} \pi \rho d_p^3 f(d_p) d(d_p)}. \quad (26)$$

Table 1  
Parameters used in the process model

Parameter	Value
$A_c/A_t$	8.0
$A_e/A_t$	2.0
$\eta_g^*$	$5 \times 10^{-5}$ kg/m s
$\lambda_g^*$	0.08 W/m K
Barrel diameter	1.0 cm
Barrel length	0.2 m
Spray distance	0.3 m

Table 2  
Simulation results of gas dynamics in the internal flow field— $P = 9.0$  bar and  $\phi = 1.0$

	Chamber	Throat	Nozzle exit
$P$ (bar)	9.000	4.986	1.002
$u$ ( $10^3$ m/s)	—	0.871	1.552
$T$ ( $10^3$ K)	2.315	2.055	1.473
<b>M</b>	—	1.000	2.092

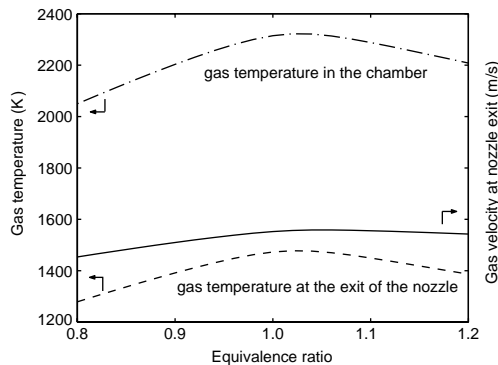


Fig. 2. Gas properties in the combustion chamber (dash-dot line: gas temperature) and at the exit of the nozzle (dashed line: gas temperature, solid line: gas velocity)— $P = 9$  bar and  $\phi = 0.8 \sim 1.2$ .

### 3. Simulation results and discussion

The oxidant and fuel used in the simulation is oxygen in an air stream and propane. The spray powder is nanocrystalline Inconel 718, whose heat capacity is 462 J/kg K, density  $9 \times 10^3$  kg/m<sup>3</sup>. The sphericity is chosen to be 1.0 for the following calculations; however, it can be readily replaced by other values. All the simulations are based on the parameters listed in Table 1. Parameters marked with \* are average values.

Table 2 shows the gas properties in the internal flow field of the HVOF gun under operating conditions  $P = 9.0$  bar and  $\phi = 1.0$ . The thermal energy of the gas phase increases as a result of the exothermic reaction in the chamber and is then partially converted into kinetic energy through the nozzle. Figs. 2 and 3 show the gas temperature in the

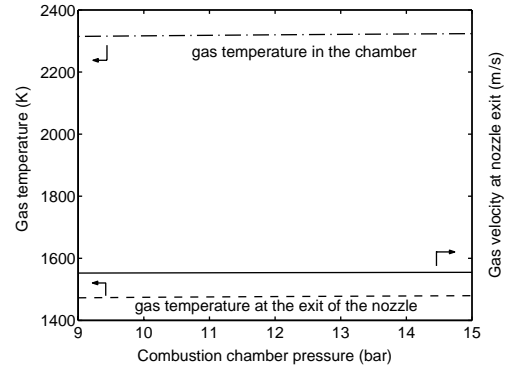


Fig. 3. Gas properties in the combustion chamber (dash-dot line: gas temperature) and at the exit of the nozzle (dashed line: gas temperature, solid line: gas velocity)— $\phi = 1.0$  and  $P = 9 \sim 15$  bar.

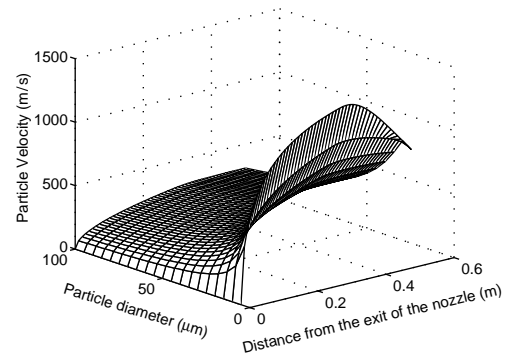


Fig. 4. Axial velocity profile of particles from the exit of the nozzle for different particle sizes— $P = 9$  bar and  $\phi = 1.0$ .

combustion chamber as well as the gas velocity and temperature at the exit of the nozzle under different operating conditions. In Fig. 2, we fix the chamber pressure at 9 bar and change the equivalence ratio from 0.8 to 1.2. It is found that in the equivalence ratio range of interest, the gas velocity at the exit of the nozzle changes very little compared to the change in the gas temperature. As the equivalence ratio increases from 0.8 to 1.2, the gas temperature at the exit of the nozzle increases initially, reaching its maximum value 1477 K at equivalence ratio slightly above 1.0, and then decreases. A similar phenomenon is also observed for the gas temperature in the combustion chamber. From these it can be concluded that fuel combustion under near stoichiometry conditions generates more thermal energy and achieves higher gas temperature. In Fig. 3, we keep equivalence ratio constant at 1.0 and change pressure from 9 to 15 bar. It can be seen that gas temperature in the combustion chamber as well as gas velocity and gas temperature at the exit of the nozzle do not change in the chamber pressure range of interest.

Figs. 4 and 5 display the axial velocity and temperature of particles with different sizes along the flow field. It can be seen that all the particles with different sizes are accelerated during passage of the barrel and part of the supersonic free

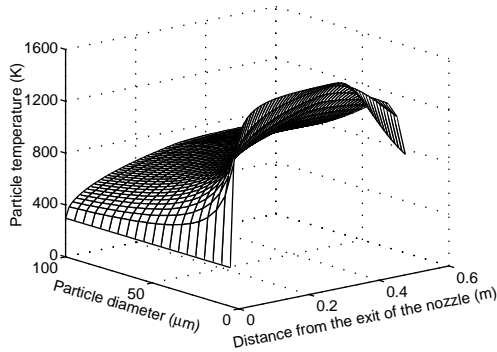


Fig. 5. Axial temperature profile of particles from the exit of the nozzle for different particle sizes— $P = 9$  bar and  $\phi = 1.0$ .

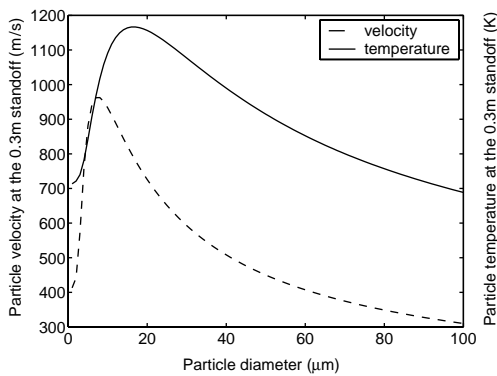


Fig. 6. Particle velocity and temperature at 0.3 m standoff as a function of particle size under operating conditions— $P = 9$  bar and  $\phi = 1.0$ .

jet (where their velocities are less than that of the combustion gas), and are then decelerated as they reach the same velocity as that of the gas. However, fine particles change their velocities/temperatures more easily than coarser ones because of their smaller momentum/thermal inertia. Referring to Eq. (21), the characteristic time scales for particle motion and heating ( $\sigma_p$  and  $\omega_p$ ) are both proportional to the square of particle size, which implies coarse particles are much more difficult to be accelerated as well as decelerated than finer ones. Although fine particles tend to attain high velocities and temperatures during flight, they are unable to maintain these high velocities and temperatures. On the contrary, their velocities and temperatures decay rapidly to follow the gas stream. For example, a particle with diameter  $5 \mu\text{m}$  attains velocity and temperature as high as about  $1300 \text{ m/s}$  and  $1554 \text{ K}$  during flight. However, its velocity and temperature decrease rapidly. For particles of even smaller size, their velocity decay even more sharply, which explains why very small size particles are not suitable for thermal spraying. For particles with large size, the velocity and temperature profiles become nearly flat after they reach the same velocity of the gas, which implies that the driving forces for motion and heating are too small to change their velocities and temperatures.

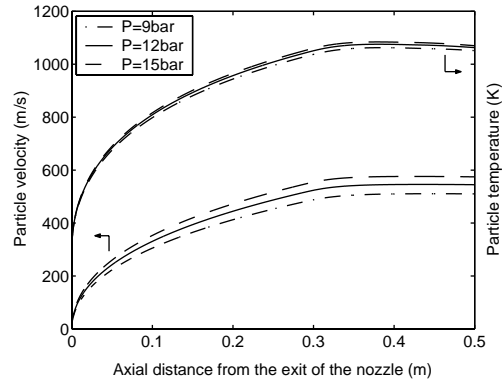


Fig. 7. Velocity and temperature profiles for particle with size  $d_p = 40 \mu\text{m}$  under operating conditions  $\phi = 1.0$  and different chamber pressures  $P = 9, 12$  and  $15$  bar.

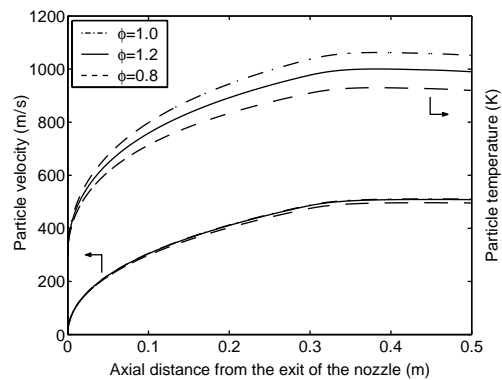


Fig. 8. Velocity and temperature profiles for particle with size  $d_p = 40 \mu\text{m}$  under operating conditions  $P = 9$  bar and different equivalence ratios  $\phi = 0.8, 1.0$  and  $1.2$ .

To better understand these phenomena, Fig. 6 shows the particle velocity and temperature at the 0.3 m standoff versus particle size. As particle diameter increases, both particle velocity and temperature increase first, and then decrease gradually. The fact that the maximum values of both velocity and temperature correspond to the medium particle sizes implies that particle size of the feedstock is one of the key parameters deciding coating quality and motivate controlling average particle velocity and temperature.

Figs. 7 and 8 show the influence of chamber pressure and equivalence ratio on velocity and temperature profiles of a single particle with  $d_p = 40 \mu\text{m}$ . In Fig. 7, we fix the equivalence ratio and vary the chamber pressure. As the chamber pressure increases, both particle velocity and particle temperature increase. However, particle velocity is more sensitive to chamber pressure than particle temperature. In Fig. 8, we change the equivalence ratio with constant chamber pressure. While the particle temperature decreases as the equivalence ratio departs from 1, the particle velocity changes very little.

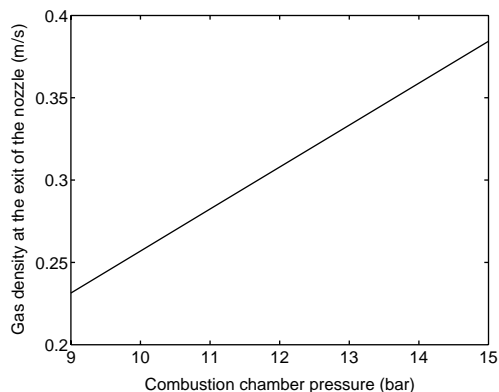


Fig. 9. Gas density at the exit of the nozzle— $\phi = 1.0$  and  $P = 9\text{--}15$  bar.

Table 3

Volume-based average particle velocity and temperature at the 0.3 m spray distance.

$P$ (bar)	$\phi$	$\bar{v}_p$ ( $10^3$ m/s)	$\bar{T}_p$ ( $10^3$ K)
9.0	0.8	0.551	0.919
9.0	1.0	0.572	1.057
9.0	1.2	0.569	0.993
12.0	1.0	0.603	1.062
15.0	1.0	0.630	1.065

From these results it can be concluded that the particle velocity is primarily influenced by the combustion chamber pressure and the particle temperature depends on the equivalence ratio, which is in good agreement with available experimental data (Swank et al., 1994a; Swank, Fincke, Haggard, Irons, & Bullock, 1994b). As we mentioned before, although chamber pressure has a minimal influence on gas velocity, it does influence particle velocity because, the drag force on particle depends strongly on gas density, which, in turn, depends on chamber pressure.

While Fig. 3 shows that chamber pressure does not affect gas velocity, the strong effect of chamber pressure on particle velocity is not unexpected. This is because chamber pressure influences gas density, and thus, particle velocity (Eq. (15)). Fig. 9 shows the gas density at the exit of the nozzle as a function of the chamber pressure. The gas density is nearly proportional to the chamber pressure.

Table 3 shows the volume-based average velocities and temperatures for particles with  $d_{10} = 15 \mu\text{m}$ ,  $d_{50} = 35 \mu\text{m}$  and  $d_{90} = 77 \mu\text{m}$  at the point of impact on substrate under five different operating conditions. The same conclusion as above can be drawn for the relationship of combustion chamber pressure and fuel/oxy ratio and particle velocity and particle temperature. Note that combustion chamber pressure is dependent on the total flow rate of air and fuel (Eq. (11)), so it is possible to control the particle velocity

and temperature at the point of impact on substrate by manipulating the total flow rate and the relative flow rate of oxygen and fuel, respectively.

In summary, a fundamental mathematical model was applied to model and analyze the HVOF thermal spray processing of nanostructured coatings. The conclusions of the modeling study were used to formulate the control problem of the HVOF process, accounting for the effect of powder size distribution, as the one of regulating the velocity and temperature of particles at the impact on substrate (these are the two variables that directly influence coating microstructure, which in turn, determine coating thermal and mechanical properties) by manipulating the total flow rate and the relative flow rate of air and fuel. The reader may refer to (Li & Christofides, 2002) for results on controller design and implementation on the process model, as well as to (Chiu & Christofides, 1999; Chiu & Christofides, 2000; El-Farra, Chiu, & Christofides, 2001; Christofides, 2002) for results on model-based control of particulate processes using nonlinear population balances.

## Notation

$a_{ij}$	number of element $j$ in species $i$
$A$	cross section area, $\text{m}^2$
$A'_p$	surface area of particles, $\text{m}^2$
$A_p$	projected area of particles, $\text{m}^2$
$b_j$	number of element $j$ in each molecule of reactants
$Bi$	Biot number
$c_p$	heat capacity at constant pressure, J/mol K
$c_v$	heat capacity at constant volume, J/mol K
$C_D$	drag coefficient
$d$	diameter, m
$F$	cumulative volume or weight function
$G$	Gibbs Energy, J/mol K
$h$	heat transfer coefficient, J/m K
$H$	Enthalpy, J/mol
$l$	number of chemical elements in the reactive system
$L_{pc}$	potential core length, m
$m$	mass, kg
$\bar{M}$	molecular weight, kg/mol
$\mathbf{M}$	mach number
$Nu$	Nusselt number
$P$	pressure, Pa
$PP$	particle properties
$Pr$	Prandtl number
$R$	gas constant, 8.314 J/mol K
$Re$	Reynolds number
$\Delta t$	time interval, s
$T$	temperature, K
$v$	velocity, m/s
$x$	axial distance, m

## Greek letters

$\varphi$	equivalence ratio
$\xi$	stoichiometric coefficient
$\mu$	chemical potential, J/mol, or mean of Gaussian distribution
$\gamma$	adiabatic constant
$\rho$	density, kg/m <sup>3</sup>
$\eta$	viscosity, kg/m s
$\sigma^2$	variance of Gaussian distribution
$\lambda$	thermal conductivity, W/m K
$\tau_p$	characteristic time for particle motion, s
$\omega_p$	characteristic time for particle heating, s

## Superscripts and subscripts

$a$	ambient condition
$c$	combustion end of the chamber
$e$	exit
$g$	properties related to gas
$i, j$	index
inj	injection interface of the chamber
$p$	properties related to particles
pr	products
re	reactants
st	stoichiometric condition
$t$	nozzle throat
$\emptyset$	standard condition
-	average

## Acknowledgements

Financial support for this work from a 2001 ONR Young Investigator Award is gratefully acknowledged.

## References

- Bird, R. B., Stewart, W. E., & Lightfoot, E. N. (1960). *Transport phenomena*. New York, USA: Wiley.
- Cheng, D., Trapaga, G., McKelliget, J. W., & Lavernia, E. J. (2001a). Mathematical modeling of high velocity oxygen fuel thermal spraying: An overview. *Key engineering materials*, 197, 1–25.
- Cheng, D., Xu, Q., Trapaga, G., & Lavernia, E. J. (2001b). The effect of particle size and morphology on the in-flight behavior of particles during high-velocity oxyfuel thermal spraying. *Metallurgical and Materials Transactions B*, 32, 525–535.
- Cheng, T. S., Wehrmeyer, J. A., Pitz, R. W., Jarrett, O., & Northam, G. B. (1994). Raman measurement of mixing and finite-rate chemistry in a supersonic hydrogen-air diffusion flame. *Combustion and Flame*, 99, 157–173.
- Chiu, T., & Christofides, P. D. (1999). Nonlinear control of particulate processes. *A.I.Ch.E. Journal*, 45, 1279–1297.
- Chiu, T., & Christofides, P. D. (2000). Robust control of particulate processes using uncertain population balances. *A.I.Ch.E. Journal*, 46, 266–280.
- Christofides, P.D. (2002). *Model-based control of particulate processes*. Particle Technology Series (228pp.). Netherlands: Kluwer Academic Publishers.
- Crow, E. L., & Shimizu, K. (1988). *Lognormal distributions: Theory and applications*. New York, USA: Marcel Dekker.
- Crowe, C. T., & Stock, D. E. (1976). A computer solution for two-dimensional fluid-particle flows. *International Journal for Numerical Methods in Engineering*, 10, 185–196.
- El-Farra, N. H., Chiu, T., & Christofides, P. D. (2001). Analysis and control of particulate processes with input constraints. *A.I.Ch.E. Journal*, 47, 1849–1865.
- Ganser, G. H. (1993). A rational approach to drag prediction of spherical and nonspherical particles. *Powder Technology*, 77, 143–152.
- Geankoplis, C. J. (1993). *Transport processes and unit operations* (3rd ed.). New Jersey, USA: Prentice-Hall.
- Gordon, S., & McBride, B.J. (1994). *Computer program for calculation of complex chemical equilibrium compositions and applications*. NASA Reference Publication 1311. Cleveland, Ohio, USA: Lewis Research Center.
- Jiang, L. Y., & Sislian, J. P. (1998). Velocity and density measurements in supersonic high-temperature exhaust plumes. *AIAA Journal*, 36, 1216–1222.
- Lau, M. L., Jiang, H. G., Nuchter, W., & Lavernia, E. J. (1998). Thermal spraying of nanocrystalline Ni coatings. *Physica Status Solidi A—Applied Research*, 166, 257–268.
- Lavernia, E. J., & Wu, Y. (1996). *Spray atomization and deposition*. New York: Wiley.
- Li, M., & Christofides, P.D. (2002). Feedback control of HVOF thermal spray process accounting for powder size distribution. *Journal of Thermal Spray Technology*, in press.
- Pawlowski, L. (1995). *The science and engineering of thermal spraying coatings*. Chichester, England: Wiley.
- Roberson, J. A., & Crowe, C. T. (1997). *Engineering fluid dynamics* ((6th ed.)). New York, USA: Wiley.
- Swank, W.D., Fincke, J.R., Haggard, D.C., & Irons, G. (1994a). HVOF gas low field characteristics. In *Proceedings of the seventh national thermal spray conference*(pp.313–318). Boston, MA.
- Swank, W.D., Fincke, J.R., Haggard, D.C., Irons, G. & Bullock, R. (1994b). HVOF particle flow field characteristics. In *Proceedings of the seventh national thermal spray conference* (pp.319–324). Boston, MA.
- Tawfik, H. H., & Zimmerman, F. (1997). Mathematical modeling of the gas and powder flow in HVOF systems. *Journal of Thermal Spray Technology*, 6, 345–352.
- Tellkamp, M. L., Lau, A., & Lavernia, E. J. (1997). Thermal spraying of nanocrystalline inconel 718. *Nanostructured Materials*, 9, 489–492.
- Yang, X., & Eidelman, S. (1996). Numerical analysis of a high-velocity oxygen-fuel thermal spray system. *Journal of Thermal Spray Technology*, 5, 175–184.